Geotechnical Aspects of Underground Construction in Soft Ground – Elshafie, Viggiani & Mair (eds)

Interaction between a newly excavated underground ramp and deep existing tunnels

A. Afshani, G. Hassan & H. Akagi
Department of Civil Engineering, Waseda University, Tokyo, Japan

K. Endou
Metropolitan Expressway Co, Tokyo, Japan

ABSTRACT: The close underground excavations inevitably become a common issue in large cities. The proximity of new excavation to existing structures changes the stress-strain regime of soil and can impose a considerable amount of load on nearby structures. A recent excavated case of an underground ramp that eases the access from underground tunnels to aboveground roads provided the chance to study proximity underground excavation and its effect on nearby structures. The ramp was excavated from the ground surface using an earth pressure balanced machine and after passing of a spiral route, it approaches and then connects to a deep existing target tunnel. The lining deformation of the target tunnel monitored before and after the passing of the excavation machine through several monitoring sections along the excavated ramp. The results of the previously performed beam-spring model related to this close excavation are presented. The proximity case of underground constructions is also simulated numerically and verified with measurement results. The verified numerical model is employed to predict the changes in the horizontal earth pressure acts on the target tunnel before and after passing of the machine in the last monitoring section of the ramp when the ramp and target tunnel are almost parallel. The results showed that among the horizontal earth pressure and internal structural forces in the target tunnel, the amount of bending moment changes as large as 35% by close excavation of nearby new tunnel.

1 INTRODUCTION

New excavation nearby to existing structures becomes a challenging issue in cities as it changes the stress-strain regime of soil and impose extra internal forces on nearby structures. The interaction between the newly constructed tunnel and the existing underground structure was studied in past years by numerical and experimental means (Ghaboussi & Ranken 1977; Soliman et al. 1993; Addenbrooke & Potts 2001; Chehade & Shahrour 2008; Wang et al. 2019; Afshani et al. 2020). Chehade and Shahrour (2008) indicated there is no significant interaction effect for distance more than 3D between tunnels which D is tunnel diameter. Wan et al. (2016) studied field instrumentation of the characteristic of the ground surface response due to tunneling in the proximity of existing structures in London Clay. In their study, vertical and horizontal surface ground displacements measured at an instrumented site in Hyde Park during the passage of two EPBMs have been analyzed and discussed. The extensive interpretation is done by comparing the settlement trough from the field reading to the Gaussian curve. Most of the intensive field observations are taken using various methods, such as precise leveling, total stations, and micrometer sticks. Ng et al. (2015) evaluated the impact of new tunnel construction on nearby existing tunnels by performing a series of three-dimensional centrifuge model tests and numerical calculations in dry sand. They concluded that the stress relief caused by the new tunnel not only led to a reduction in the vertical stress at the invert but it also resulted in substantial stress reduction at the spring line of the existing tunnel. Afshani et al. (2020) reviewed the effect of close underground excavations for tunnels having elliptical-shaped cross-section, especially in coarse-grain soil. In this study, it is demonstrated that the influence distance of close tunneling in the case of elliptical cross-section is approximately 4D where D is the tunnel minor diameter.

To the best knowledge of authors, there is no interaction study between tunnels with clear distance between tunnels less than 0.15D which D is the tunnel diameter. In this paper, excavation of an underground ramp using an earth pressure balance shield machine in a curved alignment in both vertical and horizontal

DOI: 10.1201/9781003355595-64

directions is discussed. The ramp is excavated from the ground surface along a path with a spiral route and approaches and then connect to a deep existing target tunnel. The lining deformation of a target tunnel monitored before and after the passing of the excavation machine through several monitoring sections along the excavated ramp. The results of the previously performed beam-spring model related to this close excavation is presented in the form of generated internal forces in the target tunnel. This tunneling cases is also simulated numerically and verified with measurement results. The verified numerical model is employed to predict the changes in the horizontal earth pressure and internal forces of target tunnel lining before and after passing of the machine in the last monitoring section of the ramp when the ramp and target tunnel are almost parallel.

2 MEASUREMENT DATA

2.1 *Site introduction*

To study proximity excavation, measurement data from an excavation site of a tunneling case in the south of Tokyo is used in this study. It is an underground ramp that creates the access from underground tunnels to aboveground roads. It is a part of a project called north highway ring road which includes highway and underground tunnels. Along the underground tunnels, several exit and entrance ramp were used to increase accessibility between tunnels and aboveground highway roads. The ramps were excavated from the ground surface using an earth pressure balanced machine and after passing of a spiral route, it approaches and then connects to a deep existing target tunnel. Here, one of the ramps called A ramp with a length of 459.8 m and a total number of 316 rings is used. Figure 1 shows the top view of the site and location of A ramp. Figure 2 shows the transverse cross-section at the location of section 5 shown in Figure 1. Top surface soil layers in the site are mainly loam (Lm), clay (Dc) and sand (Ds), with standard penetration test (SPT) values between 5 to 15. Under these layers, there are sand (Ks) and sandy mudstone (Kms, Km) deposits with large SPT value. The A ramp has a diameter and thickness of 9.9 m and 35 cm respectively. The ramp was excavated using a shield machine with the length and diameter of 10.845 m and 10.13 m respectively. There are two existing large-diameter tunnels (ETL and ETR tunnels shown in Figure 2) with overburden of nearly 50 m, a diameter of 12.3 m and a thickness of 40 cm located in fine sandy soil (Ks). The A ramp connects to the existing tunnel on the left, hereafter called ETL, after section 5 (the connection part has not been shown.). The ramp A mainly passes through the Dc and Ks layers. The in-situ and laboratory tests are done to obtain parameters of each layer. Table 1 lists the geotechnical parameters of each soil layer.

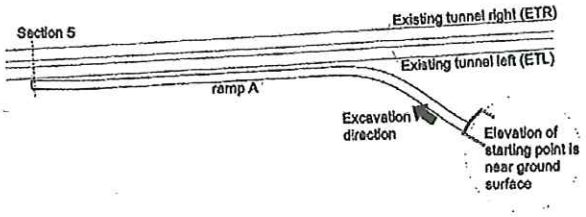

Figure 1. The general plan of the site.

2.2 *Measurement data*

At the end part of A ramp where it connects to the main tunnel ETL, in addition to the section 5 shown in Figure 1, 10 other monitoring sections

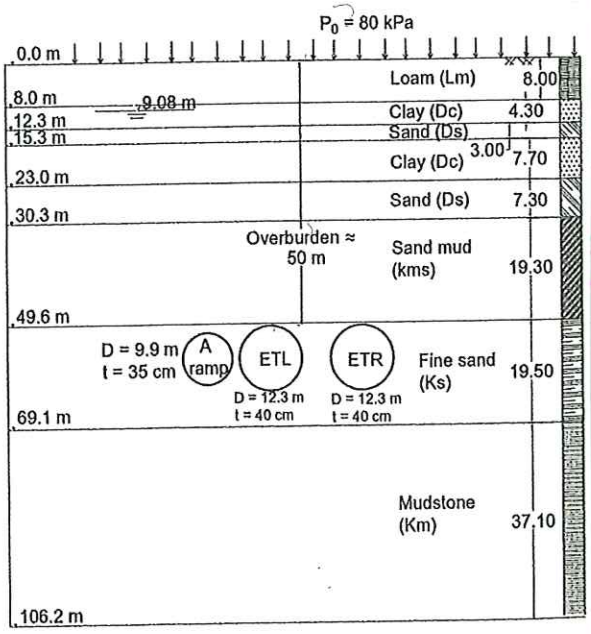

Figure 2. Details of transverse section 5.

Table 1. Soil layer parameters obtained from in-situ and laboratory tests and concrete lining properties.

Layers	Nspt	γ	E	c	ϕ	ν
Units		kN/m^3	MPa	kPa	°	-
Loam (Lm)	15	14	7.8	54	0	0.45
Clay (Dc)	5	15.5	19	160	0	0.4
Gravel (Ds)	8	18.5	20	48	34	0.3
Sandy Mud (Kms)	> 50	19	500	1800	11	0.3
Sand (Ks)	> 50	19.5	78	75	42	0.3
Mudstone (Km)	> 50	18.5	450	2000	7	0.3
Concrete lining A -ramp	-	26	39000	-	-	0.17
Concrete lining ETL, ETR	-	26	33000	-	-	0.17

Nspt is the value obtained from Standard Penetration Test, γ is wet unit weight, E is elastic modulus, c is cohesion, ϕ is internal friction angle and ν is Poisson ratio.

are considered to observe the close construction effect. The 10 surveying lines each with three stations of A, B, and C are monitored with surveying instruments. The stations A and C are located in the crown and spring line and station B is located between them.

Figure 3 shows the top view of connection part and also a cross-section of survey line 1 when clearance between two tunnels is approximately less than 0.15D (the clearance is 1.413 m and diameter of A ramp is D = 9.9 m). The illustrated numbers along A ramp in Figure 3 are ring numbers (316 rings in total). The advancement of shield machine in the ramp is expressed by ring numbers. The length of rings along ramp changes as the ramp is not straight. The vertical movement at station A in crown and horizontal displacement at station C in the spring line are important and their results are discussed here. Figure 4 shows vertical displacement of station A in the ETL tunnel at survey lines 1, 4, and 8 recorded at the entire of the time when the shield machine moves along the A ramp. Locations of survey lines 1, 4, 8 and also section 5 are demonstrated in Figure 3. It can be seen that upon arrival of the machine in A ramp, the crown of the ETL tunnel (station A) moves down by a maximum of 6 mm. Figure 5 also shows horizontal displacement of the ETL tunnel spring line (station C) at survey lines 1, 4, and 8. At the time of machine arrival in A ramp to the vicinity of survey lines, the spring line of ETL tunnel

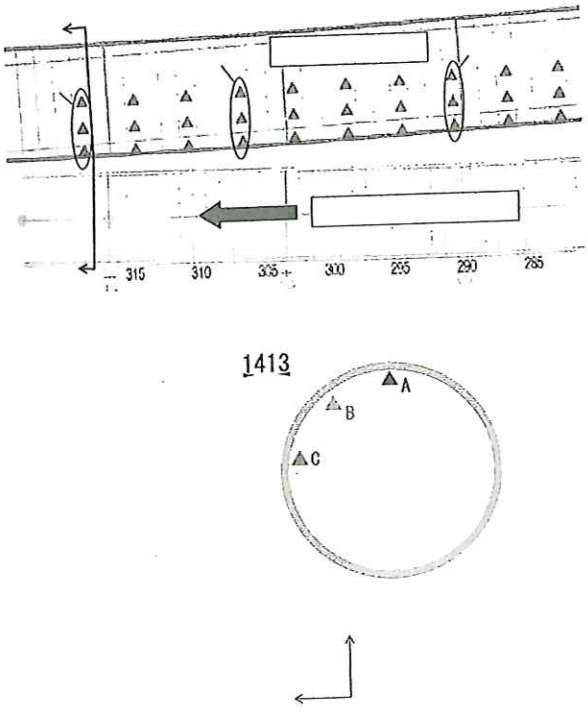

Figure 3. (Top) Plan view, and (bottom) cross-sectional view of the survey line 1 at end part of ramp A and ETL tunnel.

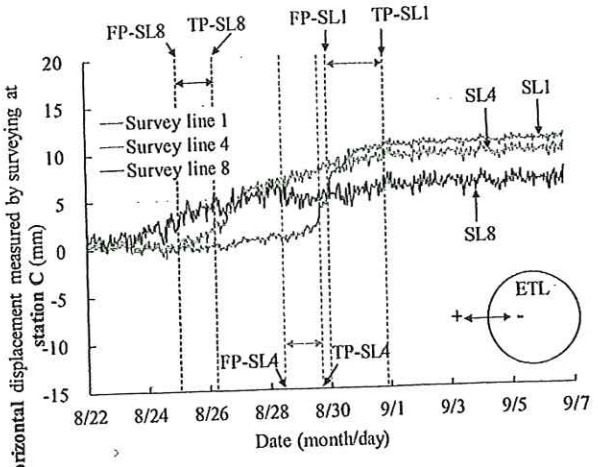

FP: The time that machine Face passes the survey line.
TP: The time that machine Tail passes the survey line.
SL: Survey Line.

Figure 4. Vertical displacement of station A at survey lines 1, 4, and 8.

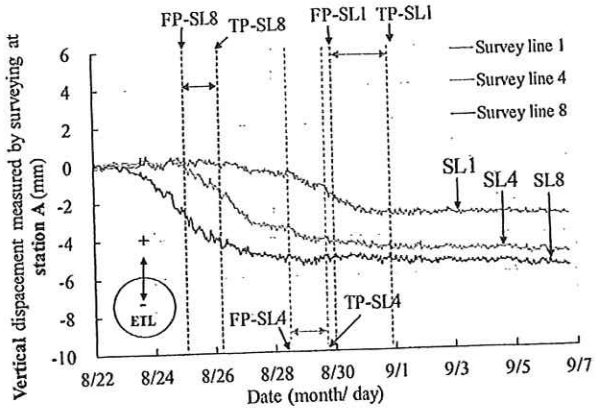

FP: The time that machine Face Passes the survey line.
TP: The time that machine Tail passes the survey line.
SL: Survey Line

Figure 5. Horizontal displacement of station C at survey lines 1, 4, and 8.

(station C) displaces toward A ramp by more than 10 mm. By approaching of machine head toward survey lines, no noticeable displacements in the lining of the ETL tunnel are found which indicates that the magnitude of face pressure is equal or less than in-situ soil and water pressures. The measurement data indicates that due to the excavation of A ramp, and probably inducing of some percentages of stress-relaxation in soil around A ramp, the soil and lining are drawn toward the gap spaces around excavated area in A ramp. The maximum horizontal displacement at the ETL spring line is larger than vertical crown displacement as the lining spring line is closer to A ramp.

Figure 6 shows the schematic of the overall measured response of the existing main tunnel ETL to the

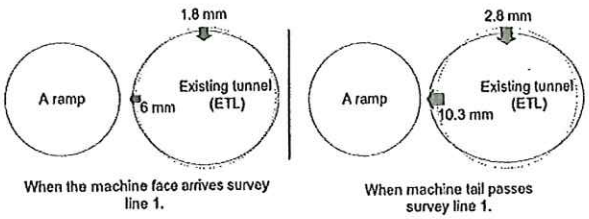

Figure 6. Overall measured response of ETL to tunnel excavation along A ramp.

tunnel excavation along A ramp. Figure 7 shows the shield machine speed and ring number in which face of machine locates (ring 270 ~ ring 316) by date of excavation. According to Figure 7, rate of machine advancement changes between 15 to 20 mm per minutes (21.6 to 28.8 m per day) and in the last few rings, it drops to 7.4 to 15 mm per minutes (10.65 to 21.6 m per day). On date 8/27 (Sunday), excavation is interrupted and speed of machine at the start of the next day declines. Figure 8 shows correlation between speed of the shield machine and horizontal displacements of the ETL at stations C of all survey lines (survey line 10 to survey line 1 as illustrated in Figure 3-top). This correlation is expressed in terms of survey line numbers and date of excavation. The direction of excavation is from survey line 10 toward survey line 1. As machine approaches end of the ramp, horizontal displacement of ETL shows increasing trend, and speed of machine decrease. It should be also noted that not only the speed of excavation, but also the distance between ramp A and

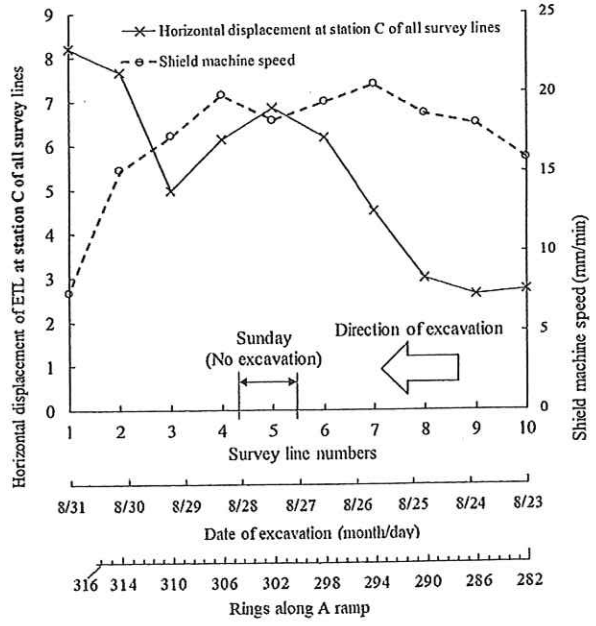

Figure 7. Ring number that machine face locates (R 270 ~ R316) and rate of machine advancements by date of excavation.

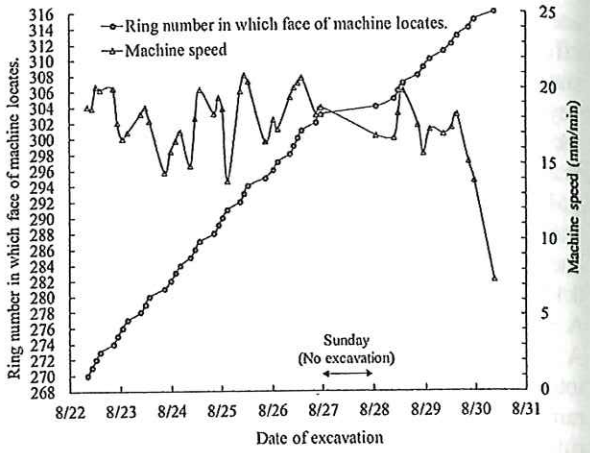

Figure 8. Measurement data of (left) horizontal displacement of ETL at station C of all survey line, (right) machine speed by date of excavation and numbers of rings along A ramp.

ETL is influential on the horizontal displacement (the net distance between external diameter of ETL and ramp decreases).

3 BEAM-SPRING MODEL

The beam-spring model is used for structural calculation of the tunnel lining in transverse and longitudinal directions. The member forces of segmental rings in the transverse direction is calculated by knowing the amounts of load and characteristics of reinforced concrete lining. The segmental rings are modeled as a beam with rotational and shear springs. Figure 9 shows the schematic of the beam-spring

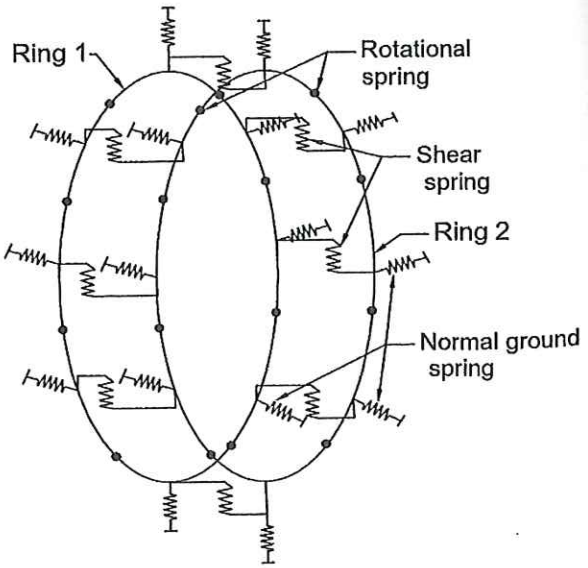

Figure 9. Schematic of beam-spring model for two neighbor rings.

model for two neighbor rings and Table 2 lists the parameters employed in this model. In Table 2, K_v represents axial ground spring, K_m shows rotational spring between segment and segment, and K_s is shear spring between ring and ring. The K_v coefficient is obtained from the value of the Standard Penetration Test of Ks soil in listed in Table 1 and the correlation proposed by Tunnel Structural Design Specification of Metropolitan Expressway (2008). The K_s coefficient is obtained from an equation recommended by the Railway Technical Research Institute (2006) as follow:

$$K_s = \frac{192EI}{(2b)^3} \quad (1)$$

where E = elastic modulus of bolt between ring to ring, I = moment of inertia of bolt section, b = is segment width of ETL (= 2 m). The value for K_m is obtained from the literature. The model is used to examine the structural behavior of ETL tunnel lining under the loads of self-weight, soil and water pressure, and the extra loads originated from machine operation in A ramp. The self-weight, and soil and water pressures are calculated readily using properties of soil layers and lining specifications.

Figure 10 shows the general imposed loads on a target tunnel (ETL) when the machine face and tail passes along a nearby tunnel. It shows that by face passing of machine along new tunnel, lining of target tunnel is pushed toward its center by horizontal pressure of q_f, while during machine tail pass, lining is pulled by the effect of horizontal distributed pressure q_t. The extra loads due to the machine operation (q_f and q_t in Figure 10) along A ramp can be obtained by numerical analyses. The details of the numerical model are given in the next section. According to the field measurements, during the both face and tail pass of the machine, ETL lining is pulled toward A ramp and therefore, in the case of this interaction problem, direction of q_f horizontal

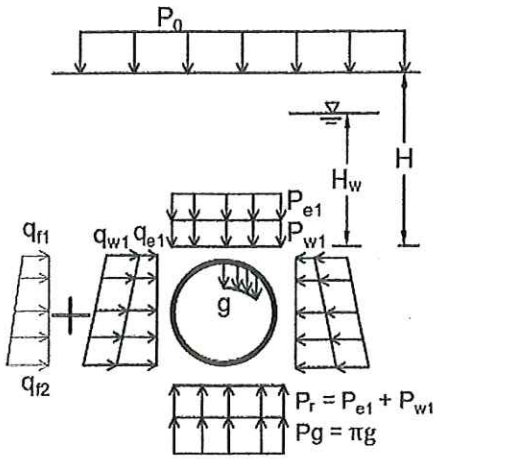

(a) Load system when machine face passes.

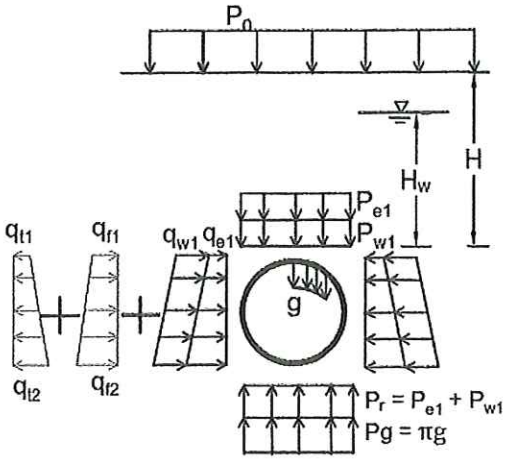

(b) Load system when machine tail passes.

Figure 10. Load system on beam-spring model when (a) machine face passes, and (b) when machine tail passes.

pressure should be opposite of the one shown in Figure 10 (a). To consider the effect of machine face and tail pass, some degree of stress-relaxations is applied. The amount of relaxation is decided based on the amount of deformation in the lining of the ETL tunnel. The amount of stress-relaxation is discussed in the next section. The values of q_{f1}, q_{f2}, q_{t1} and q_{t2} loads are read and used as an input loads in beam-spring model. After performing analyses in the beam-spring model, the maximum and minimum bending moment and corresponding values of axial force per ring are listed in Table 3.

Table 2. Beam-spring model parameters for existing left tunnel.

Parameters	Unit	Value
Tunnel Diameter (D_o)	m	12.3
Thickness of segment (t)	m	0.4
Width of segment (w)	m	2.0
Elastic modulus of segment (E_c)	GPa	39
Poisson ratio	υ	0.3
Axial stiffness of spring (K_v)	MN/m^3	50
Rotational stiffness of spring (K_m)	MN.m/rad	15
Shear stiffness of spring (K_s)	MN/m	79

Table 3. Results of beam-spring model on existing left tunnel.

	Axial force	Bending moment
Unit	kN/Ring	kN.m/Ring
Range of values	4710, 5343	- 373.3, +376.8

4 NUMERICAL MODELING

The plane-strain numerical model is used to study close construction effect between A ramp and ETL tunnel. The soil layer stratigraphy shown in Figure 2 and the soil and concrete lining properties listed in Table 1 are used in the model. The linear elastic with Mohr-Coulomb failure criteria and linear elastic models are used for soil layers and concrete linings respectively.

Employment of three-dimensional numerical model is more close to reality to estimate close construction effect, however, as A ramp and ETL tunnel become almost parallel nearby to section 5, here plain-strain model is used. Figure 11 shows the plain-strain numerical model. By using the model, it is intended to stimulate the lining deformation in ETL same as the one that occurred in the field (see Figure 4, 5, and 6) during the face and tail passing of shield machine through the survey line 1. After the creation of an equilibrium state under the self-weight of soil layers, ETL is excavated and its lining is installed. Then, the amount of stress-relaxation for the face and tail passing of machine are decided. These values are decided by fitting the lining deformation of ETL tunnel with the measurement values shown in Figures 4 and 5. The initial stress in the boundary of A ramp is reduced by 10% to simulated the face passage of the machine and for the tail passage of machine, another more 10% stress relaxation is applied and then lining of A ramp is installed. Figure 12 shows predicted and measured vertical displacement of station A at survey line 1 and Figure 13 indicates predicted and measured horizontal displacement of station A at survey line 1. By using the total stress relaxation of 10% and 20% in numerical model, the overall displacement values of ETL tunnel are close to the values of field measurements. According to Figure 12, the calculated vertical displacement at station A is slightly larger than the measured ones. One possible reason for this might be due to the non-uniform existence of gap and different percentage of stress-relaxation around A ramp in the field.

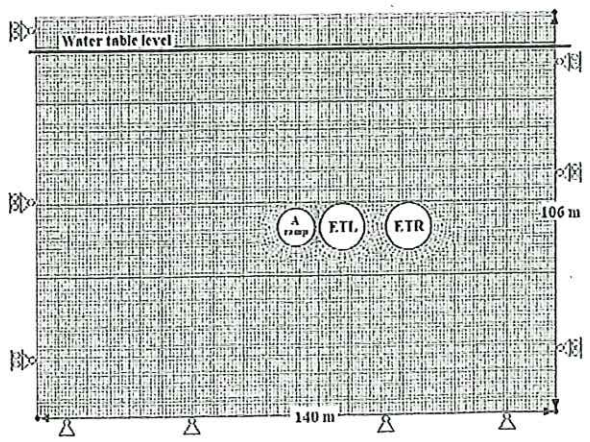

Figure 11. Numerical model.

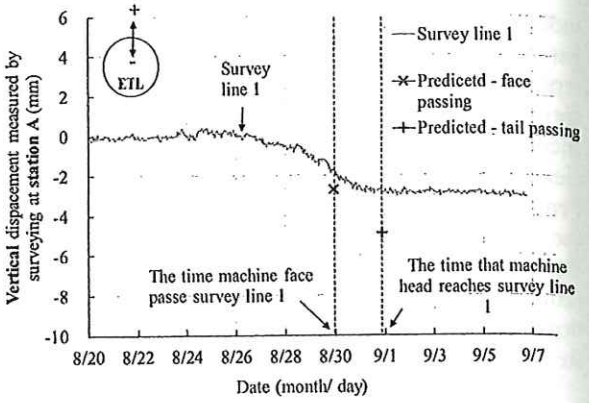

Figure 12. Predicted and measured values of vertical displacement of station A at survey line 1.

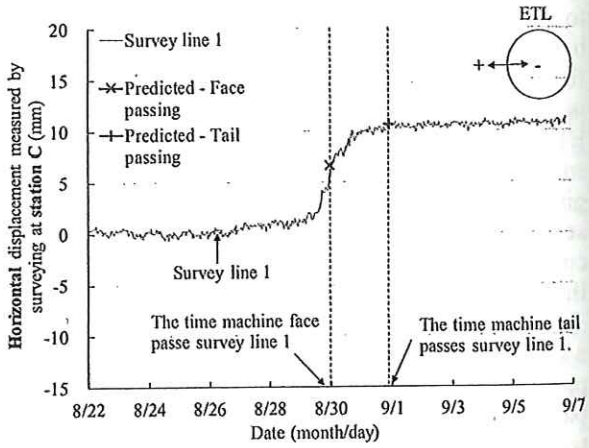

Figure 13. Predicted and measured values of horizontal displacement of station C at survey line 1.

The calibrated model is then used to examine changes of the internal forces in ETL lining and changes of horizontal soil pressure between A ramp and ETL tunnel. Figure 14 shows axial force in ETL tunnel lining at three steps (a) after ETL lining

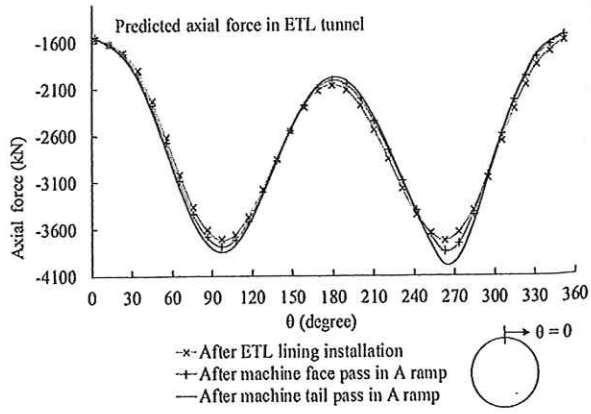

Figure 14. Predicted axial forces in ETL tunnel for various construction steps.

installation, (b) after passing of machine face in A ramp, and (c) after passing of machine tail pass in A ramp. The largest axial force occurs at both left and right spring lines and the biggest changes due to close tunneling happens at left spring line ($\theta = 270°$). At left spring line, magnitude of axial force changes from 3634 kN to 3904 kN (almost 7% increase in the amount of axial force). Figure 15 shows the distribution of bending moment in ETL tunnel lining by using the same construction steps explained previously in this part.

Maximum negative and positive bending moment occurs at 45° and 85° clockwise from crown respectively. The largest changes in the bending moment happens at the left spring line ($\theta = 270°$) from +122 to +188 kN.m (equivalent to a 35% rise in bending moment). This considerable amount of change in the bending moment due to close tunneling excavation should be considered during the design stage. The values of bending moments and axial forces listed in Table 3 from the beam spring model entail the values shown in Figure 14 and 15.

Figure 16 shows the horizontal stress in the soil between two tunnels. The soil in the pillar between two tunnels experiences large changes due to the close tunnel excavation. The σxx increases from a linear distribution in initial condition into a curved distribution after excavation and lining installation of ETL. The maximum changes occur in the soil near spring line of ETL tunnel. Then, by excavation of A ramp, the amount of horizontal stress reduces by two steps for every 10% relaxation in stress at the boundary of A ramp. The amount of reduction in horizontal stress of soil after face and tail passage of machine in A ramp is approximately 8.5%.

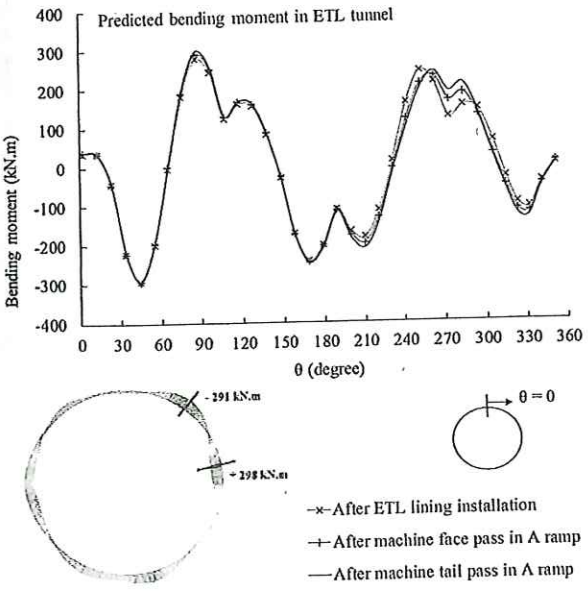

Figure 15. Predicted bending moment in ETL tunnel for various construction steps.

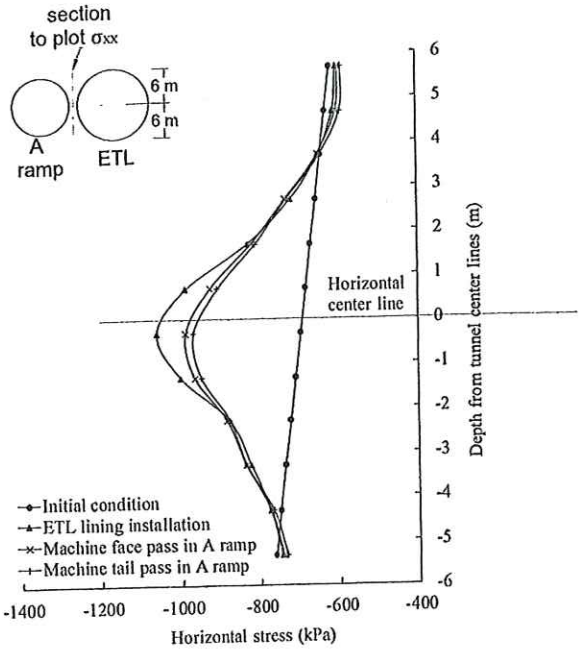

Figure 16. Predicted horizontal stress in the pillar between two tunnels.

5 CONCLUSION

In this study, the interaction between two underground tunnels with a very small distance from each other was investigated. The new tunnel is an underground ramp with curve shape alignment that was excavated from ground surface using an earth pressure balanced machine and after passing of a spiral route, it approaches and connects to a deep existing target tunnel. Numerical analyses, and results of previously performed beam-spring model were used to show the lining deformation, internal forces in target tunnel, and horizontal earth pressure distribution between two tunnels in the last monitoring section of the ramp when the ramp and target tunnel are almost parallel. The results of this study are as follow:

- According to field measurements, the pillar distance to tunnel diameter in this interaction problem is less than 0.15D and during machine face and tail pass and lining installation in new A ramp, the spring line of target tunnel is drawn toward new excavation and reaches to final value of 10.3 mm. No pushing in the lining of the target tunnel observed which indicates progressive relaxation of the stress in the soil around new excavation.
- During passage of machine face and tail along A ramp, axial force and bending moment increase by 7% and 35% respectively at left spring line of target tunnel. This considerable amount of change in the bending moment due to close tunneling excavation should be taken into account during the design stage.

- The horizontal stress of soil at pillar between two tunnels reduces by approximately 8.5% after machine pass in A ramp.

REFERENCES

Afshani, A., Akagi, H. & Konishi, S., 2020. Close construction effect and lining behavior during tunnel excavation with an elliptical cross-section. *Soils and Foundations*, 60(1), pp.28–44.

Addenbrooke, T.I. & Potts, D.M., 2001. Twin tunnel interaction: surface and subsurface effects. *International Journal of Geomechanics*, *1*(2), pp.249–271.

Chehade, F.H. & Shahrour, I., 2008. Numerical analysis of the interaction between twin-tunnels: Influence of the relative position and construction procedure. *Tunnelling and Underground Space Technology*, *23*(2), pp.210–214.

Ghaboussi, J. & Ranken, R.E., 1977. Interaction between two parallel tunnels. *International Journal for Numerical and Analytical Methods in Geomechanics*, *1*(1), pp.75–103.

Metropolitan Expressway Co. Ltd. 2008. Tunnel Structural Design Specification (Shield Tunneling).

Ng, C.W., Boonyarak, T. & Mašín, D., 2015. Effects of pillar depth and shielding on the interaction of crossing multitunnels. *Journal of Geotechnical and Geoenvironmental Engineering*, *141*(6), p.04015021.

Railway Technical Research Institute. 2006. Railway Structure Design Standard with Commentary report.

Soliman, E., Duddeck, H. & Ahrens, H., 1993. Two-and three-dimensional analysis of closely spaced double-tube tunnels. *Tunnelling and Underground Space Technology*, *8*(1), pp.13–18.

Wan, M.S.P., Standing, J.R., Potts, D.M. & Burland, J.B., 2016. Measured short-term ground surface response to EPBM tunnelling in London Clay. *Géotechnique*, *67*(5), pp.420–445.

Wang, Z., Yao, W., Cai, Y., Xu, B., Fu, Y. & Wei, G., 2019. Analysis of ground surface settlement induced by the construction of a large-diameter shallow-buried twin-tunnel in soft ground. *Tunnelling and Underground Space Technology*, *83*, pp.520–532.